Korean J. Chem. Eng., 35(2), 602-612 (2018)
DOI: 10.1007/s11814-017-0301-0

pISSN: 0256-1115
eISSN: 1975-7220

Enhancing mechanical properties of epoxy resin using waste lignin and salicylate alumoxane nanoparticles

Jamshid Behin†, Laleh Rajabi, Hamid Etesami, and Saeed Nikafshar

Faculty of Petroleum and Chemical Engineering, Razi University, Kermanshah, Iran
(*Received 4 June 2017 • accepted 25 October 2017*)

Abstract−Extracted lignin from wastewater of Kraft process and lab-made salicylate alumoxane (Sal-A) nanoparticles were used as toughening agents in epoxy matrix. Epoxy/lignin composite, epoxy/Sal-A and epoxy/lignin/Sal-Al nanocomposites with various toughening agent loadings were cured with an aromatic diamine hardener. Lignin as an available cheap material and Sal-A, as multifunctional structures, both containing numerous phenolic hydroxyls on their surfaces, were incorporated into epoxy matrix with the aim of improving thermal and some mechanical properties of the resulting composites. Both particles interacted physically (directly) and chemically (indirectly) with the epoxy chains. Simplex lattice mixture design of experiment was applied for formulation development and optimization. Fourier transform infrared spectroscopy (FT-IR), scanning electron microscopy (SEM) and transmission electron microscopy (TEM) were used to characterize the extracted lignin, Sal-A nanoparticles and synthesized composites. Differential scanning calorimetry (DSC) was used to interpret thermal curing process. The presence of lignin and Sal-A nanoparticles in the epoxy matrix decreased the exothermic peak temperature and total heat of curing reaction. In the presence of 2.5 wt% lignin and 1.875 wt% Sal-A nanoparticles, tensile strength of epoxy composites was 22.23% and 30.92% higher than that of reference (pure) epoxy resin, respectively. Vickers hardness of epoxy composites in the presence of 2.5 wt% lignin and 2.5 wt% Sal-A nanoparticles was increased by 17.41% and 15.39%, accordingly.

Keywords: Alumoxane, Epoxy, Lignin, Composite/Nanocomposite, Mechanical Properties, Thermal Properties

INTRODUCTION

Composites/nanocomposites, a new class of materials in polymer science to modify broad spectrum of polymer properties, have attracted extensie industrial attention [1]. They improve various properties of synthetic polymers such as mechanical, thermal, chemical, durability and flame retardancy [2-5]. Compared to pure polymers, composites and nanocomposites have superior properties due to enormous interfacial contacts between polymer and filler [6,7].

Due to tremendous chemical and mechanical properties, epoxy resins are one of the most interesting thermosetting polymers. They have found a wide range of applications in engineering composites, protective coatings, adhesives, molding compounds, castings, electrical and optical usage [8-11]. They have some inherent weaknesses like low thermal resistance and disability to create thin layers due to their high viscosity as well as inherently brittle and low resistance to crack propagation [12,13]. Adding filler to epoxy matrix can cover the above-mentioned drawbacks and improve properties in epoxy composites/nanocomposites [14].

Adding inorganic fillers such as SiO_2 nanoparticles in epoxy matrix provides greater hardness and elastic modulus and also increases thermal stability of epoxy nanocomposites [14]. Nanometer SiO_2/epoxy resin was prepared by means of sol-gel reaction and tensile strength, elongation at break, impact strength and bend strength of hybrid material increased compared to the pure epoxy resin [15]. Hydrothermally synthesized TiO_2 nanowire arrays were incorporated into a polyvinylidene fluoride matrix and a high energy storage density was achieved [16]. Energy storage density of nanocomposite was enhanced dispersing modified $BaTiO_3$ nanoparticles in a ferroelectric polymer matrix [17]. Small volume fraction of Ferroelectric ceramic nanofiber ($Na_{0.5}Bi_{0.5}TiO_3$) was dispersed in a polymer matrix, and a high energy density and high dielectric strength were achieved [18]. Polymeric composites with low dielectric constant and desirable thermal conductivity were prepared incorporating hyper branched polyborosilazane into bisphenol A cyanate ester matrix [19] and functionalizing hexagonal nanometer boron nitride fillers [20,21]. Ultra-high thermally conductive and rapid heat responsive polymer-based nanocomposite was produced with self-aligned graphene filler at a relatively low content [22]. Adding zirconium dioxide (ZrO_2) nanoparticles in epoxy matrix enhanced its thermal stability [23]. Carbon black nanoparticles incorporated in epoxy resin and photo-degradation of epoxy matrix was decreased significantly in 1,000 h UV-radiation [24]. Epoxy nanocomposite was reinforced with polypyrrole functionalized Fe_3O_4 magnetic nanoparticles, and its electromagnetic wave absorption was enhanced, whereas its flammability was reduced [25]. Transparent epoxy composites were prepared using low loading level of grafted thermoplastic polystyrene with epichlorohydrin, and an enhancement of the mechanical and thermal properties was achieved in the cured composites compared to the cured pure epoxy [26]. Flexural modulus and flexural strength of epoxy was

†To whom correspondence should be addressed.
E-mail: Behin@razi.ac.ir, Jamshid_Behin@yahoo.com

increased utilizing nanoclay [27]. A rigid liquid-crystalline polymer, poly{2,5-bis[(4-methoxyphenyl)oxycarbonyl]styrene}, was used as a modifier of $Na_2Ti_3O_7$ nanofibers to modulate the interfacial layer thickness. The prepared nanocomposites showed significantly different permittivity with the gradient thicknesses of polymer shell [28].

Alumoxanes are carboxylated alumina structures that have attracted great attention for their various applications and permanent stability in air and water [29]. They can be applied in different areas as catalyst components [30], polymeric nanocomposites [31], non-flammable/non-skid coatings and in lithium batteries [32]. They are synthesized from boehmite nanoparticles and carboxylic acid and are described as alumina nanostructures which surface is covered by carboxylate groups. Four types of carboxylate-alumoxanes were synthesized and characterized from boehmite nanoparticles and corresponding carboxylic acid: parahydroxybenzoatealumoxane, para aminobenzoatealumoxane, fumarate alumoxaneand salicylate alumoxane (Sal-A) [30]. Sal-A epoxy nanocomposites were found to have increased hardness [33].

Lignin is a complex chemical compound and one of the most abundant biopolymers in nature [34]. It is an amorphous and polydispersed natural polyphenols polymer (made of rigid phenyl units) with a chemical structure that distinctly differs from the other macromolecular constituents of wood [35,36]. Its chemical structure contains phenylpropane units, originating from three aromatic alcohol precursors (monolignols), p-coumaryl, coniferyl, andsinapyl alcohols [37,38]. Its high polarity and great reactivity with various chemicals is due to a variety of functional groups like aromatic and aliphatic hydroxyl, methoxyl and carbonyl. However, the molecular structure and function groups differ for the various types of lignin [39]. During the chemical pulping processes (e.g., Kraft), the partially degraded lignin is dissolved in the black liquor, from which it can be later isolated by different methods. It is a waste byproduct normally burned for heat generation [39]. However, the significant potential to use for value added products due to high toughness and good thermal resistance [40,41] makes it a suitable additive/filler for thermosetting polymers and a marvelous candidate to act as toughening agent while reacting with epoxy resins [42]. It decreases density of epoxy networks without negative effects on mechanical strengths and thermal properties [43]. It was reported that modified lignin, as a curing agent, improves toughness and adhesive shear strength of cured epoxy system compared to neat epoxy [44-46].

In the present work, incorporation of waste lignin and Sal-A as two multifunctional structures with epoxy as the polymer matrix is reported. These two particle types were chosen due to their common functional groups on their surfaces. Therefore, their contribution in interacting with the epoxy matrix as well as affecting the thermal and mechanical properties of the resulting composites could be compared.

MATERIALS AND METHODS

The epoxy resin RL 440 as a general purpose diluted diepoxide based on bisphenol-A and epichlorohydrin monomers was used as received. A low viscosity amine hardener, HY 441, was used as curing agent. Sodium hydroxide, aluminum nitrate 9-hydrate, salicylic acid and ethanol were purchased from Merck Company (Germany). Black liquor containing 43 wt% waste lignin was supplied from Kraft pulping of spruce (Choka Company, Anzali/Iran).

1. Synthesis of Sal-A Nanoparticles

20 g (0.0533 mol) aluminum nitrate ($Al(NO_3)_3{\cdot}9H_2O$) and 6.49 g (0.16225 mol) sodium hydroxide were dissolved in 50 and 30 mL distilled water, respectively. Sodium hydroxide solution was added to aluminum nitrate solution under moderate mixing using a graduated burette with a rate of 1.25 mL/min in a period of 40 min. Aluminum hydroxide ($Al(OH)_3$) was gradually precipitated as a white sediment. The mixture was then placed in an ultrasonic bath for 3 h at 25 °C to obtain a uniform mixture. The synthesized boehmite nanoparticle was put in an oven for 4 h at 220 °C, and then it was washed with distilled water and centrifuged three times and dried in an air-oven for 24 h at 60 °C to remove the impurities such as nitrate and sodium ions.

6 g of the synthesized boehmite nanoparticles and 12 g (0.0869 mol) of the salicylic acid were dissolved in 200 mL distilled water and subjected to ultrasonic irradiation for 10 min at room temperature (25±5 °C). Then the mixture was refluxed on heater stirrer at ~100 °C and atmospheric pressure for 10 h. The separated sediment was dissolved in 200 mL ethanol to neutralize unreacted acid, and centrifuged. Sal-A nanoparticles were dried at room temperature.

2. Extraction of Lignin from Black Liquor

To separate the lignin from black liquor by ultrafiltration, it is necessary to decrease its viscosity. Black liquor was diluted (volume

Table 1. Preparation epoxy system with various compositions (actuallevels), E: Epoxy, EL: Epoxy/Lignin, ES: Epoxy/Sal-A, ELS: Epoxy/Lignin/Sal-A

Sample code	Run no.	Lignin	Nano Sal-A
		wt%	wt%
E: Epoxy	1	0	0
EL_1	4	0.625	0
EL_2	9	1.250	0
EL_3	6	1.875	0
EL_4	16	2.500	0
ES_1	5	0	0.625
ES_2	2	0	1.250
ES_3	7	0	1.875
ES_4	10	0	2.500
ELS_1	11	0.625	0.625
ELS_2	3	1.250	0.625
ELS_3	8	0.625	1.250
ELS_4	18	1.875	0.625
ELS_5	19	1.250	1.250
ELS_6	12	0.625	1.875
ELS_7	14	0.833	0.833
ELS_8	13	0.417	0.417
ELS_9	15	1.667	0.417
ELS_{10}	17	0.417	1.667

ratio: 1 : 3) with an aqueous solution of acetic (50%). To remove the impurities, 100 mL diluted black liquor was poured in a dead-end filtration cell under nitrogen pressure to drive the liquor through the lab-made membrane. The membrane was made from polyethersulfone 18% containing 1% polyvinylpyrrolidone. The remaining lignin was collected and put in the oven at 35±5 °C for 24 h to dry.

3. Preparation Epoxy/Lignin and Epoxy/Sal-A Composites

The appropriate amount of epoxy resin, lignin and Sal-A nanoparticles was mixed for 2 min as indicated in Table 1 and then put in ultrasonic bath for 1 h at room temperature to obtain a homogeneous mixture. After adding the curing agent (hardener), the mixing continued for 2 min to remove gas bubbles. Then, the mixture was poured into silicon mold and cured in a pre-heated oven for 1 h at 80 °C. To complete curing reaction (post curing), temperature was increased to 100 °C for 1 h. Then, silicon mold was cooled to room temperature. The prepared composite/nanocomposites were removed from silicon mold and subjected to mechanical tests.

A mixture design of experiment (simplex lattice) was conducted using Design Expert software (version 10) to evaluate the effect of amount of epoxy (E, wt%), lignin (L, wt%) and Sal-A (S, wt%) on mechanical properties of produced nanocomposites, i.e., tensile strength, elastic modulus and elongation at break. The highest amount of particles (2.5 wt%, lignin and Sal-A nanoparticles) was considered and total 19 experimental runs were proposed as shown in Fig. 1.

The experimental run orders, corresponding sample code and weight percent of each component are illustrated in Table 1. Resin: hardener ratio was equal to 113:17 for all samples.

4. Characterization

4-1. Fourier Transform Infrared Spectroscopy (FT-IR)

FT-IR (Tensor 27, Bruker with 40 scan average at a resolution of 4 cm^{-1}) was used to characterize lignin and Sal-A nanoparticles.

4-2. Tensile Strength (TS)

Tensile strength test was conducted in accordance with ASTM D638 using Shimadzu 20KN-testig machine. Specimen dimensions of composite samples were 165×19×3.2 mm. Crosshead speed was adjusted to 2 mm/min and five specimens were prepared and tested for each sample.

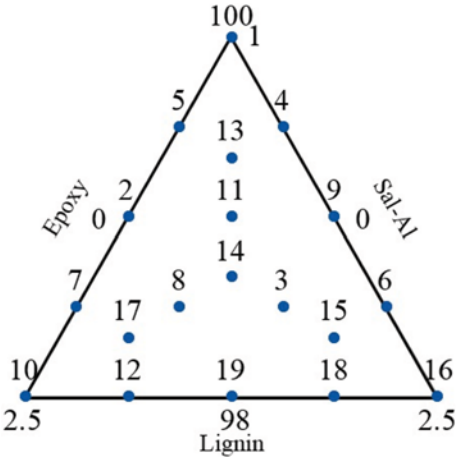

Fig. 1. Proposed experiments by simplex lattice mixture design.

4-3. Vickers Hardness Test (VK)

A micro-hardness tester (hardness tester, Model HT2A, Germany) was used to determine Vickers hardness of the composite samples in accordance with ASTM E 384-99, using a diamond indenter and 120 K_{gf} load applied for 30, 60 and 90 seconds. Specimen dimensions were 80×40×45 mm.

4-4. Differential Scanning Calorimetry (DSC)

DSC analysis (Linseis, PT10, Germany) was used to report curing information. A non-isothermal test at a heating rate of 10 °C/min under airflow rate of 200 mL/min at the temperature range 25-200 °C was performed on 5 mg of sample. This analysis was conducted on selected samples with the highest tensile strength.

4-5. TEM and FE-SEM

Synthesized boehmite and Sal-A nanoparticles were characterized by TEM (Philips CM10, high tension 100 kv). To investigate the effect of Sal-A nanoparticles and lignin on the toughness of epoxy system, fracture surfaces were analyzed using FE-SEM (Hitachi, S-4160, Japan). Samples were coated with gold vapor and FE-SEM was done at an accelerating voltage of 20.0 kV.

RESULTS AND DISCUSSION

TEM micrographs of boehmite and Sal-A nanoparticles are illustrated in Figs. 2(a) and (b), respectively. Boehmite nanoparticles with cubic orthorhombic crystal structure and particles size of 15-30 nm as well as Sal-A nanoparticles with rode shape: diameter and length in the range 40-50 nm and 0.5-1.5 μm, respectively; nanostrips: length and width 100-300 nm and 0.5-4 μm, respec-

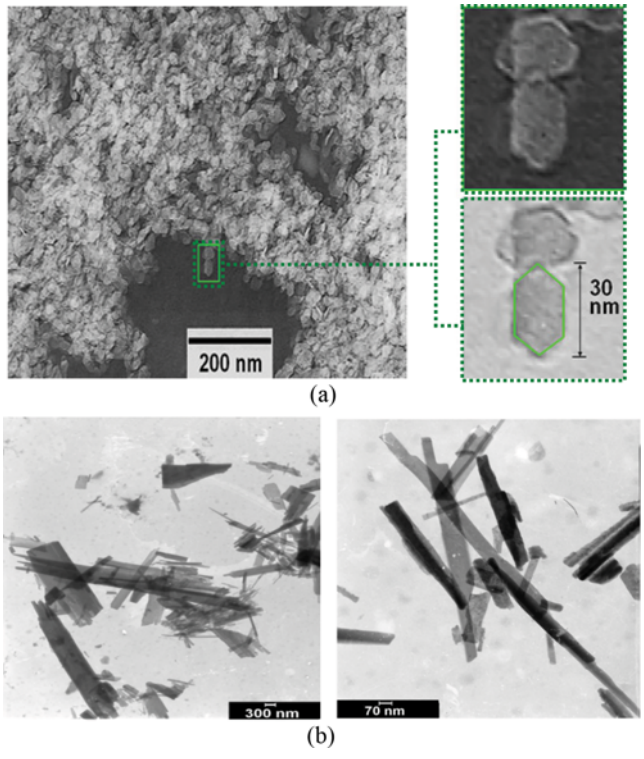

Fig. 2. TEM micrographs of nanoparticles. (a) Boehmite nanoparticles (right: higher magnification), (b) Sal-A nanoparticles (right: higher magnification).

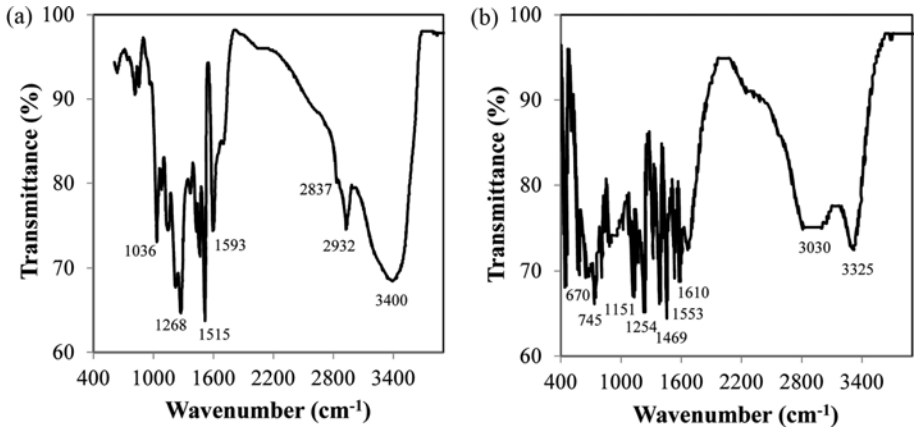

Fig. 3. FT-IR spectra. (a) Lignin, (b) Sal-A nanoparticles.

tively and nanoplates: thickness, length and width 70-100 nm, 3-4 μm and 1-3 μm, respectively, are well detected.

FT-IR spectra of lignin and Sal-A nanoparticles are given in Figs. 3(a) and (b), respectively. Vibration bonds of Al-O-Al are detected at 670 cm^{-1} and 745 cm^{-1}. Two absorption peaks at 1,151 cm^{-1} and 1,254 cm^{-1} correspond to the stretching vibrations of carboxylate C-O groups and phenolic C-O groups, respectively. Two strong absorption peaks at 1,407 cm^{-1} and 1,553 cm^{-1} belong to the symmetrical and asymmetrical stretch vibrations of carbonyl groups of the carboxylate, respectively. C=C vibration aromatic rings have absorption peaks at 1,469 cm^{-1} and 1,610 cm^{-1}. Vibration bonds at 3,030 cm^{-1} and 3,075 cm^{-1} correspond to the stretch vibrations of aromatic C-H groups and absorption peak around 3,325 cm^{-1} is assigned to phenolic OH groups. Hence, the cited absorption peaks confirm that Sal-A nanoparticles were successfully synthesized [30]. As shown in Fig. 3(b), the broad absorption peak at around 3,400 cm^{-1} corresponds to stretch vibration of O-H. Absorption peaks at 2,932 cm^{-1} and 2,837 cm^{-1}, 1,593 and 1,515 cm^{-1}, 1,268 cm^{-1} and 1,036 cm^{-1} are assigned to C-H stretching, aromatic vibrations and C-O vibrations, respectively, being in good agreement with literature [47].

It was proposed that lignin and Sal-A nanoparticles can react with the curing agent through its hydroxyl groups as follows [48]:

$$\text{Lignin-OH}+\text{H}_2\text{N-R}\rightarrow\text{Lignin-HN-R}+\text{H}_2\text{O} \quad (1)$$

and

$$\text{Sal-A-OH}+\text{H}_2\text{N-R}\rightarrow\text{Sal-A-HN-R}+\text{H}_2\text{O} \quad (2)$$

As a result, both lignin and Sal-A nanoparticles can interact with epoxy chains chemically and they become a part of the epoxy matrix.

The results of mechanical properties tests for the samples are presented in Fig. 4. All estimated data were expressed as mean± standard deviation (S.D.), and each measurement was conducted in triplicate. Computational work including design matrix, analysis of variance, fitting of the models, model validation and graphical representations (2D and 3D plots) was performed using a statistical package (Design Expert). On increasing the amount of lignin in the epoxy matrix, tensile strength increased (Fig. 4(a)). Tensile strength of sample EL_4 (2.5% lignin) was improved 22.23% compared to reference epoxy resin (E). Also, on addition of 1.875 wt% Sal-A nanoparticles to epoxy resin, tensile strength increased (46.53 MPa) about 30.92% in comparison to reference epoxy system. As mentioned, lignin and Sal-A nanoparticles are multifunctional structures, with large number of phenolic groups on their surfaces due to which they both can interact directly with the epoxy matrix through strong hydrogen bonding and also through primary interactions with the amine hardener. Adding more Sal-A nanoparticles, however, decreased tensile strength. Since, more nanoparticles were tended to aggregate. The improved tensile strengths for produced composite/nanocomposites were in agreement with epoxy composites strengthened and toughened by thermoplastic polystyrene grafted with epichlorohydrin [26]. Among epoxy/lignin samples, EL_3 (1.875 wt% lignin) had the highest elastic modulus (Fig. 4(b)). When lignin and Sal-A nanoparticles were added together in epoxy matrix in varying amounts, tensile strength and elastic modulus both increased compared to neat epoxy. Sample ELS_5 showed the highest tensile strength (44.79 MPa) with 26.03% improvement compared to reference epoxy resin. Among the different samples, epoxy/lignin (EL_3: 1.875 wt% lignin), epoxy/Sal-A nanocomposites (ES_3: 1.875 wt% Sal-A nanoparticles) and epoxy/lignin/Sal-A composites (ELS_5: 1.25 wt% lignin and 1.25 wt% Sal-A) showed a relatively high elastic modulus. These improvements are related to effective transfer of stress in the interface of epoxy matrix and additives. Therefore, toughening agents like lignin and Sal-A nanoparticles enhance elastic modulus of the corresponding composites and nanocomposites [48].

Elongation at break (%) of samples is shown in Fig. 4(c). With increasing the loaded amount of lignin and Sal-A nanoparticles in the epoxy matrix, elongation at break decreased, indicating that the rigidity of lignin and Sal-A nanoparticles did not accommodate the same strain as the epoxy matrix. Incorporation of lignin and Sal-A nanoparticles into epoxy matrix can toughen the epoxy network without stiffening of composite samples. The results are comparable with the ones obtained on SiO_2/epoxy resin hybrid materials prepared by means of Sol-Gel method [15] and on structural non-halogenated epoxy resin composites [49].

Fracture surface examinations of epoxy systems by SEM can reveal information regarding location and reason of failure and

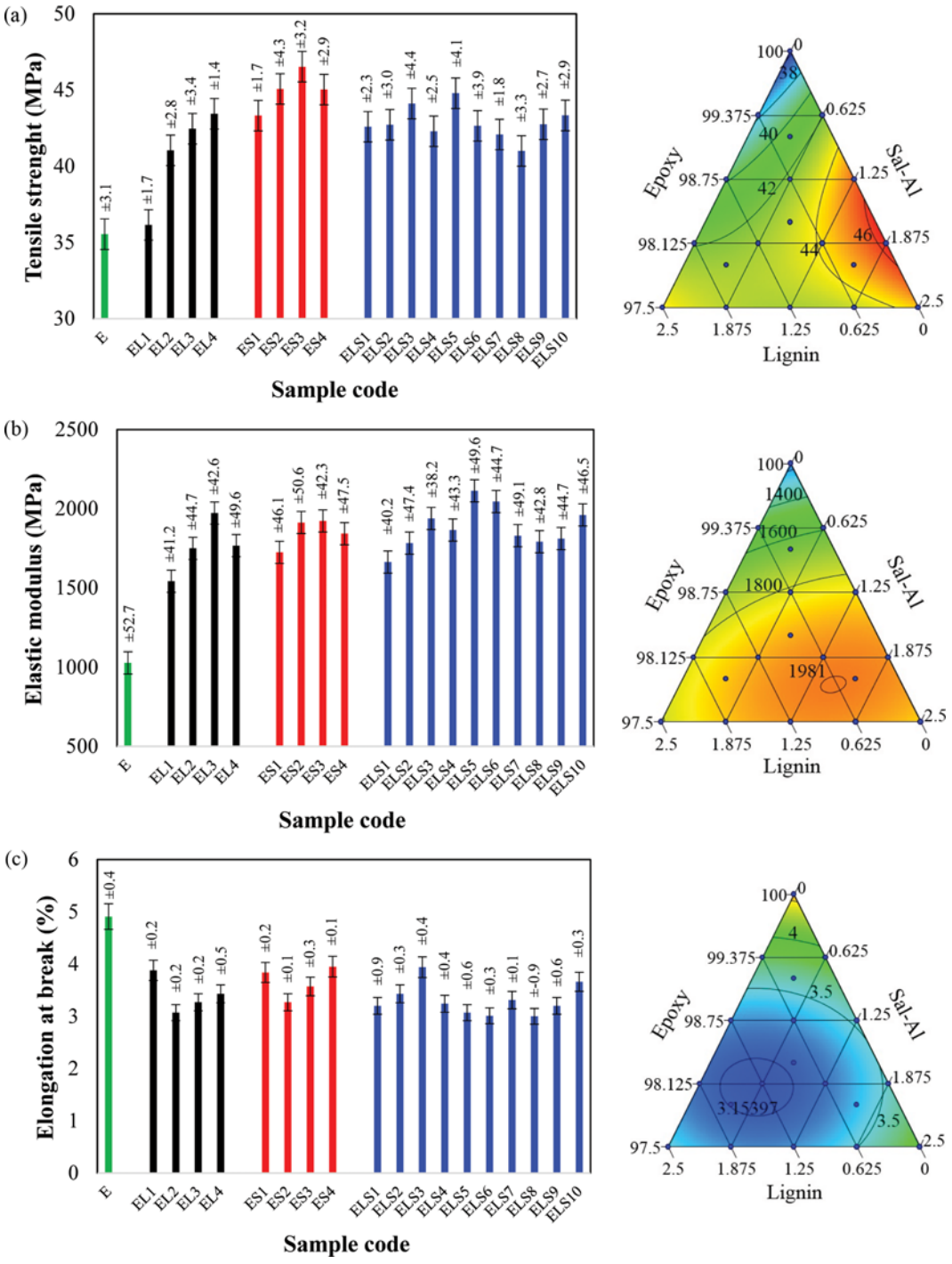

Fig. 4. Mechanical properties of the various samples and contour diagram indicating optimization of dependent variables. (a) Tensile strength, (b) Elastic modulus, (c) Elongation at break.

dispersion quality of nanoparticles and toughenners. Crack propagation and failure of filled epoxy resins are described by several known mechanisms [50]. If additives are weak, cracks likely pass through the particles that it is named as trans-particulate failure, and if the fillers are enough strong, cracks pass around them. In addition, cohesive failure of the matrix may occur [33]. The fracture surface is often classified in two distinguished regions: crack initiation zone and propagation zone. Fig. 5(a) shows SEM micrograph of the fracture surface of pure epoxy resin as reference (sample E). The cracks grew slowly in the initial stage where the smooth fracture surface was made, called mirror zone. Mist zone was followed by mirror zone, which was slightly rougher. After mist zone, the hackle zone appeared, which was a very rough surface and it was produced when cracks reached to limited speed and excess energy was dispersed in branches. It can be seen that on adding lignin and Sal-A nanoparticles, cracks were propagated

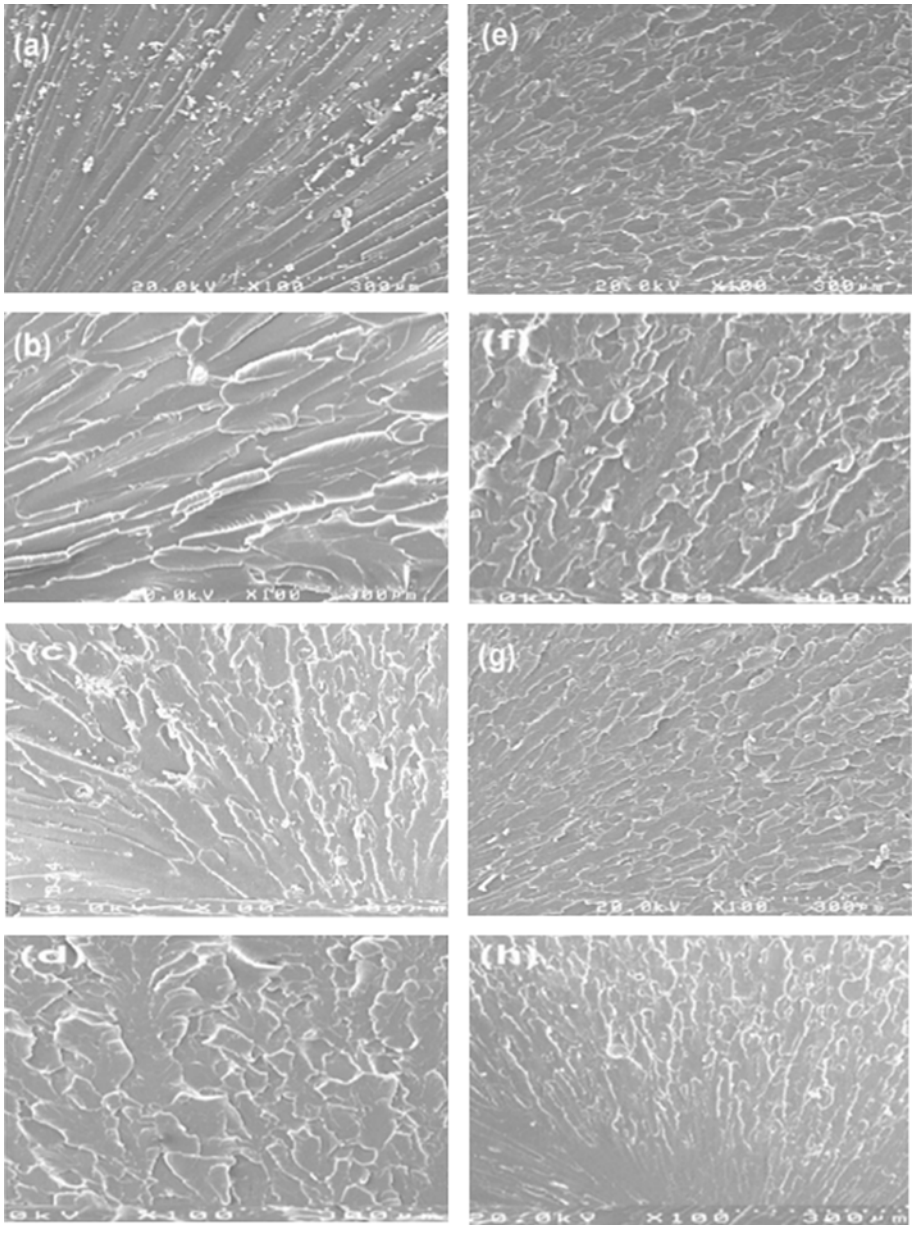

Fig. 5. SEM micrograph of some selected samples. (a) Sample E (Pure epoxy), (b) Sample EL_1, (c) Sample EL_3, (d) Sample ELS_8, (e) Sample ES_3, (f) Sample ES_4, (g) Sample ELS_5, (h) Sample ELS_2.

as growing branches throughout the fracture surface while in the pure epoxy matrix, cracks moved in straight lines (E). Lignin and Sal-A nanoparticles created branching cracks as they dispersed and could not pass through the additives on reaching them, forming branches (samples EL_1, ES_4 and ELS_2). Samples with denser branches had more enhanced mechanical properties such as EL_3, ES_3 and ELS_5 as shown in Fig. 5(c), (e) and (g), respectively, Smooth surface can be attributed to agglomeration. In epoxy/lignin/Sal-A nanocomposite samples, a smooth surface area was not detected, which means lignin and Sal-A were dispersed homogeneously throughout the polymer matrix.

SEM morphologies of Sal-Al nanoparticles, lignin (L), epoxy/Sal-A nanocomposite (ES_1), and epoxy/lignin composite (EL_1) are shown in Fig. 6(a) to (d), respectively. The selected nanocomposite/composite samples had lowest mechanical properties, among all produced ones. Sal-A and lignin both contain functional groups in their structures that enables them to interact with the epoxy matrix. These interactions may be of different types. Sal-A nanostructures may interact chemically with the amine hardener, which in turn reacts with the epoxy functionality as part of the structure of the amine hardener molecule. However, this tendency to react with the amine hardener molecules may somewhat increase the agglomeration chances of the Sal-A nanoparticles, besides the usual tendency of the nanoparticles to agglomerate, especially at higher concentrations. On the other hand, the phenolic hydroxyls on the Sal-A surfaces can also interact physically with the epoxy chains, resulting in the good dispersion of the Sal-A nanoparticles in the polymer matrix.

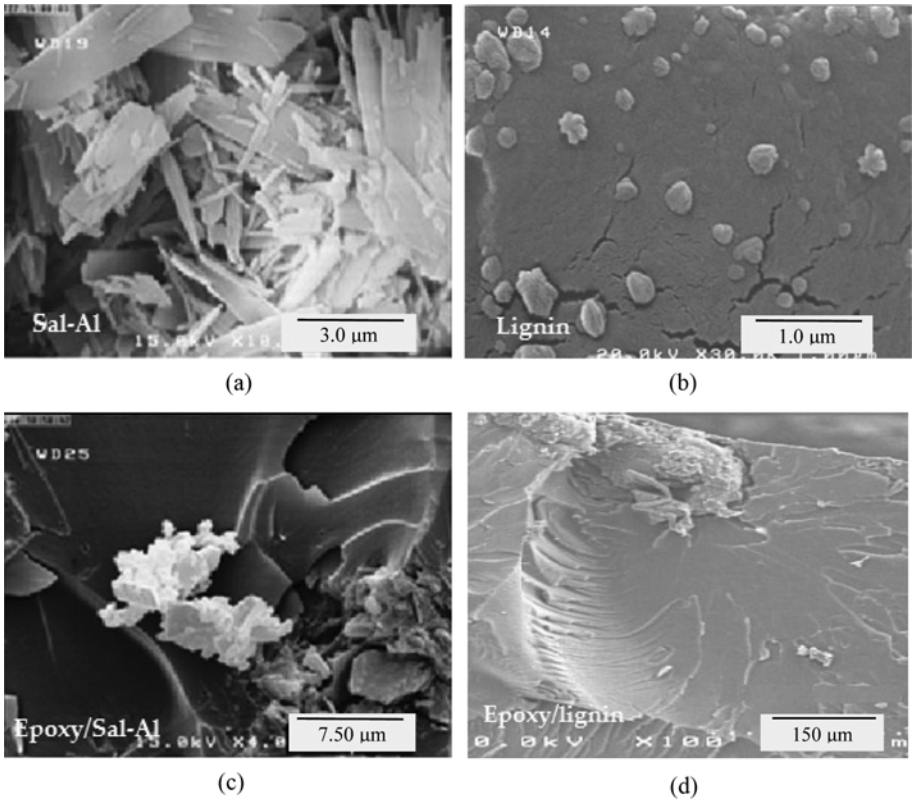

Fig. 6. SEM morphologies of typical samples. (a) Sal-A nanoparticles, (b) Lignin particles (L), (c) Epoxy/Sal-A nanocomposite (ES_1), (d) Epoxy/lignin composite (EL_1).

The tendency to agglomerate is higher for the lignin particles, as these macromolecular structures contain numerous phenol groups, as well as polar alcoholic ether groups that tend to interact among the lignin molecules. This can cause more agglomeration to occur and thus, fewer chances to interact with the epoxy chains, leading to lower extent of dispersion.

However, the phenol groups on the surface of the Sal-A nanostructures are somewhat directed inwards and are less exposed for any possible type of interaction. Whereas, the phenol groups on the surface of the lignin molecules are very numerous and exposed. Thus, the presence of both particle types in the epoxy matrix, balanced the above-mentioned positive and negative points and as the experimental results indicated, their combination with the epoxy matrix improved the overall properties of the corresponding composites.

Analysis of variance (ANOVA) was used to estimate the significance of the model and removed the non-significant terms ($p > 0.05$). The Model F-value for all responses implied the model is significant (Table 2).

The best fit equations for all the responses were obtained after removing the non-significant terms. The second-order polynomial equations for each response variable in terms of actual components are shown as follows:

$$\text{Tensile strength (MPa)} = +0.357\,E - 1.850\,L - 330.17S + 3.426\,E.S \quad (3)$$

$$\text{Elastic modulus (MPa)} = +11.536\,E - 15077.468\,L - 20710.706\,S + 157.383\,E.L + 315.555\,E.S \quad (4)$$

$$\text{Elongation at break (\%)} = +0.046\,E + 44.470\,L + 43.664\,S - 0.460\,E.L - 0.450\,E.S \quad (5)$$

A numerical optimization technique based on desirability function approach was used to optimize the compositions of formulation. However, optimization of all variables at the same time is not possible at a time because several responses may be applicable to do the same when one response may antagonize another. 3D-surface plots show the effects of variables on the response factors (Fig. 7). Optimization of investigated mechanical properties resulted in following tougher compositions: L: 0.16% and S: 1.63% for whole properties with 0.852 desirability. L: 0% and S: 1.77% for tensile strength with 0.984 desirability; L: 0.66% and S: 1.47% for elastic modulus with 0.879 desirability; L: 1.33% and S: 0.58% for elongation at breaks with 0.936 desirability. Therefore, three typical samples (EL_4, ES_3 and ELS_5) associated with reference (pure) epoxy sample (E) were selected for consecutive experiments.

Curing of epoxy based formulations was studied by DSC, which provides useful information regarding different aspects of curing reaction [51,52]. Pure epoxy resin (E) and EL_4, ES_3 and ELS_5 samples that had the highest mechanical properties were selected for DSC analysis. Non-isothermal/dynamic DSC curve of pure epoxy/hardener illustrates one exothermic peak (Fig. 8). Heat is released during curing of epoxy because of ring opening reaction. The peak temperature and total heat of curing reaction of pure epoxy system (the epoxy/hardener resin system without any filler) was 106.9 °C and 625 J/g, respectively. For sample EL_4 (2.5 wt% lignin), they

Table 2. ANOVA for tensile strength, elastic modulus and elongation at break. E: Epoxy (wt%), L: Lignin (wt%), S: Sal-A (wt%)

Source	Sum of squares	df*	Mean square	F-value	Probability>F
For tensile strength (MPa)					
Model	117.67	5	23.53	20.20	<0.0001
Linear of mixture	76.83	2	38.41	32.97	<0.0001
EL	0.00968	1	0.00968	0.00831	0.9288
ES	35.71	1	35.71	30.65	<0.0001
LS	2.45	1	2.45	2.10	0.1710
Residual	15.15	13	1.17		
Cor. total	132.82	18			
Other statistics: Std. Dev.: 1.08, Mean: 42.47, CV(%): 2.54, PRESS: 36.43, R^2: 0.8860, Adjusted R^2: 0.8421, Predicted R^2: 0.7257, Adequate precision: 17.552					
For elastic modulus (MPa)					
Model	7.760×10^5	5	1.552×10^5	11.05	0.0003
Linear of mixture	5.757×10^5	2	2.878×10^5	20.50	<0.0001
EL	75332.67	1	75332.67	5.36	0.0375
ES	1.413×10^5	1	1.413×10^5	10.06	0.0073
LS	16413.72	1	16413.72	1.17	0.2993
Residual	1.825×10^5	13	14042.04		
Cor. total	9.585×10^5	18			
Other statistics: Std. Dev.: 118.50, Mean: 1802.74, CV(%): 6.57, PRESS: 5.314×10^5, R^2: 0.8096, Adjusted R^2: 0.7363, Predicted R^2: 0.4456, Adequate precision: 12.392					
For elongation at break (%)					
Model	2.31	5	0.46	3.70	0.0266
Linear of mixture	1.10	2	0.55	4.42	0.0343
EL	0.64	1	0.64	5.16	0.0407
ES	0.62	1	0.62	4.94	0.0446
LS	0.18	1	0.18	1.40	0.2574
Residual	1.62	13	0.12		
Cor. total	3.93	18			
Other statistics: Std. Dev.: 0.35, Mean: 3.49, CV(%): 10.13, PRESS: 3.70, R^2: 0.5872, Adjusted R^2: 0.4284, Predicted R^2: 0.0577, Adequate precision: 7.443					

*Degree of Freedom, $p<0.05$ is considered as significant

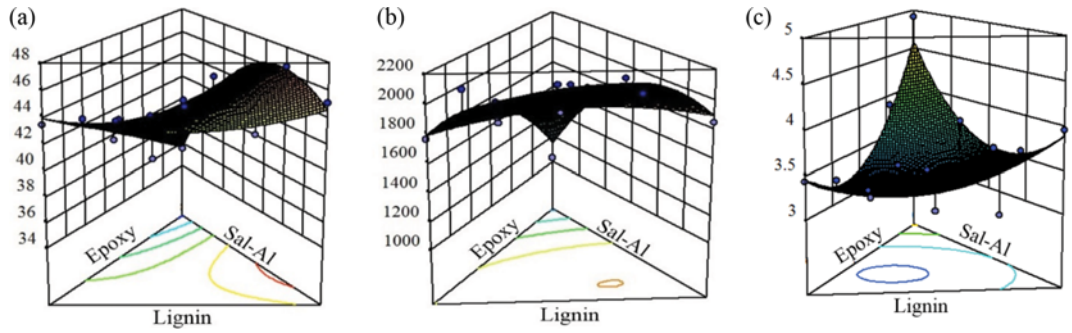

Fig. 7. 3D-surface plots showing the effects of variables on the response factors. (a) Tensile strength (MPa), (b) Elastic modulus (MPa), (c) Elongation at break (%).

reduced to 95.44 °C and 414 J/g, respectively. This reduction also occurred for sample ES_3 (1.875 wt% Sal-A) at 88.5 °C and 303 J/g and for sample ELS_5 (1.25 wt% lignin and 1.25 wt% Sal-A) at 100.6 °C and 502 J/g, respectively. These reductions of exothermic peak temperature occurred due to the presence of lignin and Sal-A nanoparticles. Lignin has hydroxyl and phenolic hydroxyl groups in its structure, and also Sal-A nanoparticles has many hydroxyl groups. It was confirmed that hydroxyl and phenolic hydroxyl groups catalyze curing reaction of epoxy resin and they act as an accelerator [53]. Therefore, the exothermic peak temperatures of

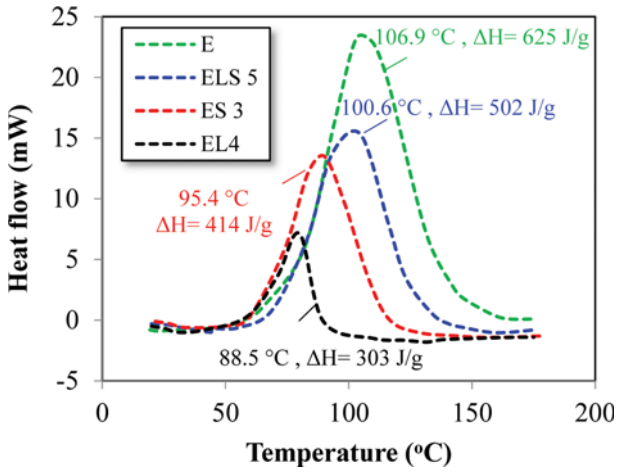

Fig. 8. DSC results for four selected samples at heating rate 10 °C/min.

samples EL_4, ES_3 and ELS_5 are less than the reference epoxy system without any additive. So, on adding lignin or Sal-A to epoxy matrix, the total heat of curing reaction was reduced, indicating that the presence of lignin and Sal-A nanoparticles decreased the extent of crosslinking. This behavior was confirmed in several studies [44,45]. It was proposed that lignin and Sal-A nanoparticles can react with the curing agent through its hydroxyl groups as reactions (1) and (2) [45], which in turn got covalently bonded to the epoxy chains. The amount of amine hydrogens that can react with epoxy rings got reduced, decreasing the crosslink density of epoxy system. Moreover, reduction of the heat of reaction can be attributed to the enhancement of viscosity of the epoxy system and decreased mobility of molecules as a result of adding lignin and Sal-A nanoparticles [33].

Hardness tests provide the time dependent flow behavior of various materials. Polymers creep at different temperatures even at room temperature. It has been indicated that hardness of polymers changes with time with the load imposed through intender, and it can be applied as an indication of the relative creep resistance of polymers. Therefore, time taken for reading hardness is essential and important. Pending the loading of polymers, low level of elastic deformation happens, which is followed by viscoelastic flow. When loading is removed, asthmatic elastic recovery happens and is followed by a time-depending recovery of the deformation. Material nature, temperature and the state of internal stress are factors that affect the recovery of viscoelastic polymers. Following equation was used to calculate Vickers hardness number (H_v):

$$H_v = 1.854\frac{F}{d^2} \tag{3}$$

where F is load (kg) and d is diagonal length (mm).

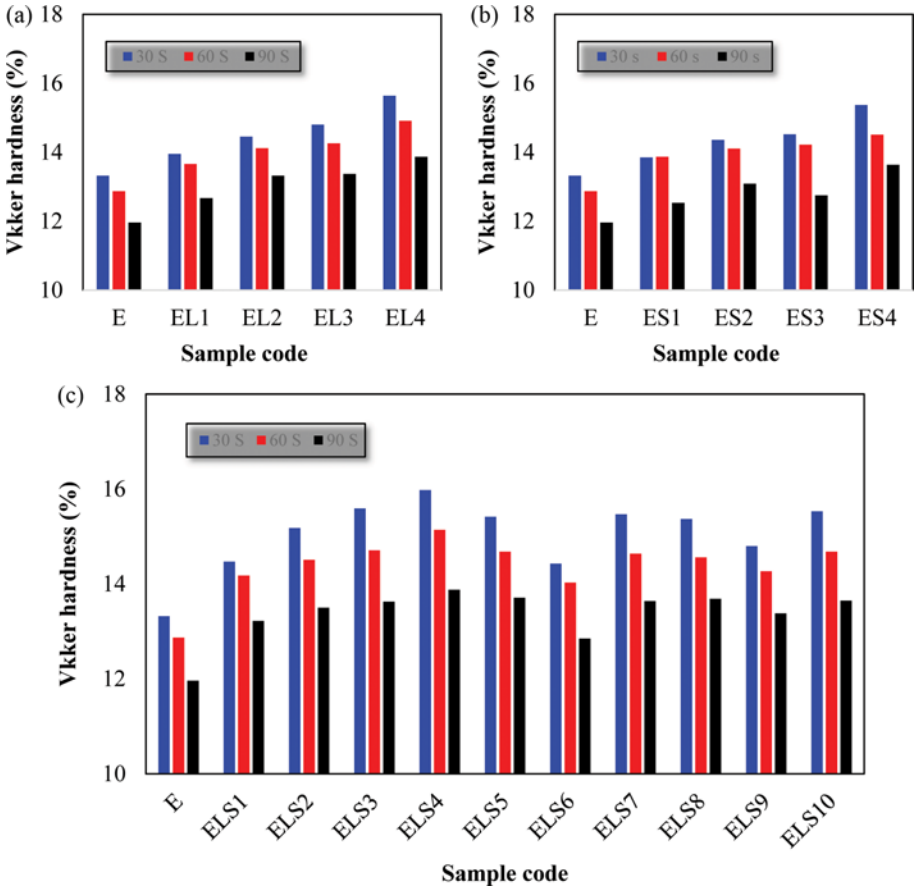

Fig. 9. Hardness of all samples. (a) Epoxy/lignin, (b) Epoxy/Sal-A, (c) Epoxy/lignin/Sal-A.

The values of Vickers hardness of pure epoxy, epoxy/lignin system, epoxy/Sal-A nanocomposite and epoxy/lignin/Sal-A nanocomposite are presented in Fig. 9(a), (b) and (c) for different toughener loading. In epoxy/lignin samples, on increasing the amount of lignin, the value of Vickers hardness was enhanced and the highest amount of Vickers hardness was obtained in 2.5 wt% lignin loaded epoxy system. In the epoxy/lignin sample (EL_4, 2.5 wt%), Vickers hardness (30 sec) was increased 17.42% compared to the reference epoxy system. As mentioned earlier, lignin is a macromolecule which contains aliphatic and aromatic components and increasing in Vickers hardness can be attributed to lignin structure. Hardness was improved due to the presence of Sal-A nanoparticles in the corresponding epoxy nanocomposites (Fig. 9(b)) with the highest value for 2.5 wt% epoxy/Sal-A sample ES_4 (30 sec) being 15.39% higher as compared to reference epoxy resin. This improvement can be related to high dispersion tendency and intermolecular interactions of Sal-A nanoparticles in epoxy matrix due to molecular structure and surface chemistry of Sal-A nanoparticles.

The effect of both lignin and Sal-A nanoparticles on the Vickers hardness is demonstrated in Fig. 9(c). It is obvious that the greatest Vickers hardness (15.98 Hv) is related to 1.25 wt% lignin and 1.25 wt% Sal-A nanoparticles (ELS_4), which is 19.97% more than reference epoxy resin. Generally, the mentioned improvements in different samples (epoxy/lignin, epoxy/Sal-A and epoxy/lignin/Sal-A) are related to the nature of lignin and Sal-A nanoparticles. Lignin and Sal-A interact with epoxy matrix not only through physical interactions, but also they react with epoxy matrix chemically.

According to obtained result from various tests, both lignin and Sal-A nanoparticles had positive effects on epoxy matrix properties. Tensile strength and Vickers hardness increased significantly in the presence of lignin and Sal-A nanoparticles, and DSC information showed that the mentioned additives lowered peak temperature and total heat of curing reaction. In addition, SEM images of fracture surface proved the positive effect of lignin and Sal-A nanoparticles.

CONCLUSIONS

Lignin and salicylate alumoxane (Sal-A) were incorporated into the epoxy/amine hardener polymer matrix to study their effect on thermal and some mechanical properties of the resulting composites. The least number of experiments were performed using simplex lattice mixture design to optimize the mechanical properties of nanocomposites as response factors. Lignin and Sal-A nanoparticles had remarkable impacts on curing reaction of epoxy system, and peak temperature and total heat of curing reaction were decreased. Tensile strength of epoxy was increased (22.23%) with 2.5 wt% lignin and (30.92%) with 1.875 wt% Sal-A nanoparticles. Enhancements of ~17% and ~15% in Vickers hardness (30 s) of the epoxy system were achieved with 2.5 wt% lignin and 2.5 wt% Sal-A, respectively. Both particle types proved to have increased toughness of the epoxy/hardener resin system.

REFERENCES

1. F. Hussain, M. Hojjati, M. Okamoto and R. E. Gorga, *J. Compos. Mater.*, **40**, 1511 (2006).
2. I. Armentano, M. Dottori, E. Fortunati, S. Mattioli and J. Kenny, *Polym. Degrad. Stabil.*, **95**, 2126 (2010).
3. P. Cosoli, G. Scocchi, S. Pricl and M. Fermeglia, *Micropor. Mesopor. Mater.*, **107**, 169 (2008).
4. H. Ma, Z. Xu, L. Tong, A. Gu and Z. Fang, *Polym. Degrad. Stabil.*, **91**, 2951 (2006).
5. J. K. Pandey, K. R. Reddy, A. P. Kumar and R. Singh, *Polym. Degrad. Stabil.*, **88**, 234 (2005).
6. A. P. Kumar, D. Depan, N. S. Tomer and R. P. Singh, *Prog. Polym. Sci.*, **34**, 479 (2009).
7. N. Sheng, M. C. Boyce, D. M. Parks, G. Rutledge, J. Abes and R. Cohen, *Polymer*, **45**, 487 (2004).
8. Y. Si, Z. Guo and W. Liu, *ACS Appl. Mater. Inter.*, **8**, 16511 (2016).
9. J. Michels, R. Widmann, C. Czaderski, R. Allahvirdizadeh and M. Motavalli, *Compos. Part B-Eng.*, **77**, 484 (2015).
10. B. Zhang, M. Johlitz, A. Lion, L. Ernst, K. Jansen, D.-K. Vu and L. Weiss, 17th International Conference on Thermal, Mechanical and Multi-Physics Simulation and Experiments in Microelectronics and Microsystems (EuroSimE), *IEEE* (2016).
11. C. P. Wang, *Polymers for Electronic and Photonic Application*, Elsevier Science (2013).
12. A. M. El Saeed, M. A. El-Fattah and M. Dardir, *Prog. Org. Coat.*, **78**, 83 (2015).
13. F. El-Tantawy, K. Kamada and H. Ohnabe, *Mater. Lett.*, **56**, 112 (2002).
14. R. Khan, M. R. Azhar, A. Anis, M. A. Alam, M. Boumaza and S. M. Al-Zahrani, *J. Coat. Technol. Res.*, **13**, 159 (2016).
15. J. Gu, Q. Zhang, H. Li, Y. Tang, J. Kong and J. Dang, *Polym-Plast. Technol.*, **46**, 1129 (2007).
16. D. Zhang, W. Liu, L. Tang, K. Zhou and H. Luo, *Appl. Phys. Lett.*, **110**, 133902 (2017).
17. H. Luo, D. Zhang, C. Jiang, X. Yuan, C. Chen and K. Zhou, *ACS Appl. Mater. Inter.*, **7**, 8061 (2015).
18. H. Luo, J. Roscow, X. Zhou, S. Chen, XHan, K. Zhou, D. Zhang and C. R. Bowen, *J. Mater. Chem. A*, **5**, 7091 (2017), DOI:10.1039/c7ta00136c.
19. J. Gu, S. Xu, Q. Zhuang, Y. Tang and J. Kong, *IEEE T. Dielect. El. In.*, **24**, 784 (2017).
20. X. Yang, L. Tang, Y. Guo, C. Liang, Q. Zhang, K. Kou and J. Gu, *Composites A*, **101**, 237 (2017).
21. J. Gu, Y. Guo, X, Yang, C. Liang, W. Geng, L. Tang, N. Li and Q. Zhang, *Composites A*, **95**, 267 (2017).
22. W. Zhao, J.Kong, H. Liu, Q. Zhuang, J. Gu and Z. Guo, *Nanoscale,* **8**, 19984 (2016).
23. S. Halder, M. Goyat and P. Ghosh, *High Perform. Polym.*, **28**, 697 (2015).
24. A. Ghasemi-Kahrizsangi, J. Neshati, H. Shariatpanahi and E. Akbarinezhad, *Prog. Org. Coat.*, **85**, 199 (2015).
25. J. Guo, H. Song, H. Liu, C. Luo, Y. Ren, T. Ding, M. A. Khan, D. P. Young, X. Liu, X. Zhang, J. Kong and Z. Guo, *J. Mater. Chem. C*, **5**, 5334 (2017).
26. H. Gu, C. Ma, C. Liang, X. Meng, J. Gu and Z. Guo, *J. Mater. Chem.* C, **5**, 4275 (2017).
27. Y. Zhou, M. Hosur, S. Jeelani and P. K. Mallick, *J. Mater. Sci.*, **47**, 5002 (2012).

28. H. Luo, C. Ma, X. Zhou, S. Chen and D. Zhang, *Macromolecules*, **50**, 5132 (2017), DOI:10.1021/acs.macromol.7b00792.
29. A. A. Derakhshan and L. Rajabi, *Powder Technol.*, **226**, 117 (2012).
30. A. R. Barron and S. J. Obrey, *Supra-molecular alkylalumoxanes*, US Patent, 6,322,890 B1 (2001).
31. T. S. Halbach and R. Mülhaupt, *Polymer*, **49**, 867 (2008).
32. A. S. Mistry, Q. P. Pham, C. Schouten, T. Yeh, E. M. Christenson, A. G. Mikos and J. A. Jansen, *J. Biomed. Mater. Res. A.*, **92**, 451 (2010).
33. L. Rajabi, M. Marzban and A. A. Derakhshan, *Iran. Polym. J.*, **23**, 203 (2014).
34. D. Glennie and J. McCarthy, Chemistry of lignin, McGraw-Hill, New York (1962).
35. C. I. Simionescu, V. Rusan, M. M. Macoveanu, G. Cazacu, R. Lipsa, C. Vasile, A. Stoleriu and A. Ioanid, *Compos. Sci. Technol.*, **48**, 317 (1993).
36. R.-C. Sun, *Cereal straw as a resource for sustainable biomaterials and biofuels: Chemistry, extractives, lignins, hemicelluloses and cellulose*, Elsevier, Beijing (2010).
37. E. Dorrestijn, L. J. Laarhoven, I. W. Arends and P. Mulder, *J. Anal. Appl. Pyrol.*, **54**, 153 (2000).
38. W. Boerjan, J. Ralph and M. Baucher, *Annu. Rev. Plant Biol.*, **54**, 519 (2003).
39. S. Laurichesse and L. Avérous, *Prog. Polym. Sci.*, **39**, 1266 (2014).
40. C. Aouf, J. Lecomte, P. Villeneuve, E. Dubreucq and H. Fulcrand, *Green Chem.*, **14**, 2328 (2012).
41. J. Behin and N. Sadeghi, *International Journal of Recycling of Organic Waste in Agriculture*, **5**, 289 (2016).
42. A. Mirmohseni-Namin, S. Nikafshar and F. Mirmohseni, *RSC Adv.*, **5**, 53025 (2015).
43. C. L. Sherman, R. C. Zeigler, N. E. Verghese and M. J. Marks, *Polymer*, **49**, 1164 (2008).
44. W. Liu, R. Zhou, H. L. S. Goh, S. Huang and X. Lu, *ACS Appl. Mater. Inter.*, **6**, 5810 (2014).
45. D. Feldman and M. Khoury, *J. Adhes. Sci. Technol.*, **2**, 107 (1988).
46. D. Feldman, D. Banu, A. Natansohn and J. Wang, *J. Appl. Polym. Sci.*, **42**, 1537 (1991).
47. K. Pandey, *J. Appl. Polym. Sci.*, **71**, 1969 (1999).
48. D. Feldman and D. Banu, *J. Polym. Sci. A1*, **26**, 973 (1988).
49. J. Gu, J. Dang, Y. Wu, C. Xie and Y. Han, *Polym-Plast Technol. Eng.*, **51**, 1198 (2012).
50. B. Wetzel, F. Haupert and M. Q. Zhang, *Compos. Sci. Technol.*, **63**, 2055 (2003).
51. D. S. Achilias, M. M. Karabela, E. A. Varkopoulou and I. D. Sideridou, *J. Macromol. Sci. A.*, **49**, 630 (2012).
52. W. Chow, S. Grishchuk, T. Burkhart and J. Karger-Kocsis, *Thermochim. Acta*, **543**, 172 (2012).
53. E. Petrie, Epoxy adhesive formulations, McGraw Hill Professional (2005).